



Relationships Between Ground-Motion Intensity Measures and Earthquake-Induced Permanent Slope Displacement Based on Numerical Analysis

Mao-Xin Wang, Dian-Qing Li, and Wenqi Du(✉)

State Key Laboratory of Water Resources and Hydropower Engineering Science,
Institute of Engineering Risk and Disaster Prevention, Wuhan University,
Wuhan 430072, People's Republic of China
wqdu309@whu.edu.cn

Abstract. In engineering applications, the permanent displacement (D) commonly serves as a useful indicator of the seismic performance of slopes. When developing empirical displacement models as a function of ground-motion intensity measures (IMs), the IMs that are best correlated to D are preferred. On the other hand, the predictability of IMs, in terms of the standard deviations using ground motion models, is also of concern in developing D models. This study aims to: (1) investigate the efficiency of IMs in developing D models for a cohesive-frictional slope based on numerical analysis; and (2) compare the means and standard deviations of randomized D by considering uncertainties in predicting both the IMs and D via Monte Carlo simulation (MCS). A total of 10 scalar IMs and 38 vector-IMs, are employed to develop D models. The results indicate that the spectral acceleration at a degraded period of the soil layer ($SA(1.5T_{s,layer})$) and Arias intensity (IA) are the two most efficient scalar IMs. Additionally, the vector-IMs consisting of [IA, spectrum intensity] and [IA, mean period] are the two most efficient vectors. The MCS results illustrate that the rankings for standard deviations of D models and total standard deviations (i.e., including ground motion variability) may be considerably different. The results are also found to be dependent on earthquake magnitudes and site conditions. This study could provide guidance on the development of numerical-based D models especially within a probabilistic seismic slope displacement analysis framework.

Keywords: Seismic slope performance · Numerical analysis · Intensity measure · Displacement prediction · Model variability

1 Introduction

Evaluating the seismic stability of slopes is an important task of geotechnical engineers. The performance-based permanent displacement analysis has attracted increasing attention in assessing the seismic safety of slopes, as usually conducted by the Newmark-type sliding block procedures [1–3]. Such procedures that approximately estimate the

earthquake-induced permanent slope displacement (D) are particularly useful for preliminary screening-level analyses and regional landslide hazard mapping. For assessing the seismic performance of important slopes such as those involved in critical projects, the numerical stress-deformation analysis is necessary to provide a more accurate estimate of the slope performance [4].

The probabilistic displacement hazard approach has been well developed to estimate the hazard-consistent D [5–7]. Recently, this approach has been improved with the numerical slope displacement analysis [8]. As a key component, the relationship between one or multiple ground motion (GM) intensity measure (IMs) and D (i.e., higher efficiency) are recommended as predictor variables. Therefore, it is of interest to investigate the efficiency of different IMs. However, most of the existing studies were based on the Newmark-type procedures (e.g., [9]), so the findings and conclusions may not hold for the numerical cases [8, 10]. Also, the efficiency rankings of various IMs may be dependent on slope materials, slope geometry, etc. Hence, more research efforts should be devoted to this topic.

This study aims to: (1) investigate the performance of IMs in developing D models for a cohesive-frictional slope based on numerical analysis; and (2) compare the means and standard deviations of D for these models considering uncertainties in predicting both the IMs and D via Monte Carlo simulation (MCS). The remaining part of this paper starts with a description of the procedure employed, followed by the slope model development and comparative results.

2 Procedure for Seismic Slope Displacement Analysis

The seismic slope displacement analysis procedure includes the following steps.

- (i) Select GM acceleration-time series, and compute their IMs of interest. The GMs selected should cover a wide range of the earthquake magnitude (M), rupture distance (R), and shaking intensity, etc.
- (ii) Perform dynamic analysis for the slope model using each of the GMs to obtain D .
- (iii) Develop D models based on the obtained data of D . The trend of $\ln D$ versus $\ln IM$ (i.e., in natural logarithmic scale) is fitted via one of the following formulas:

$$\ln D = \mu_{\ln D} + \varepsilon_{\ln D} \cdot \sigma_{\ln D} = a_1 \ln IM_1 + a_0 + \varepsilon_{\ln D} \cdot \sigma_{\ln D} \quad (1)$$

$$\ln D = \mu_{\ln D} + \varepsilon_{\ln D} \cdot \sigma_{\ln D} = a_1 \ln IM_1 + a_2 \ln IM_2 + a_0 + \varepsilon_{\ln D} \cdot \sigma_{\ln D} \quad (2)$$

where D is in units of cm; a_0 , a_1 , and a_2 are regression coefficients; $\varepsilon_{\ln IM}$ denotes a standard normal variable; $\sigma_{\ln D}$ is the model-specific standard deviation, so $\ln D$ follows the normal distribution with mean of $\mu_{\ln D}$ and standard deviation of $\sigma_{\ln D}$.

- (iv) Perform MCS to generate N_{IM} samples of the correlated IMs. The probability distribution of $\ln IM$ is described by the associated ground motion model (GMM) with the following general expression [11]:

$$\ln(IM) = \mu_{\ln IM}(M, R, \text{etc.}) + \varepsilon_{\ln IM} \cdot \sigma_{\ln IM} \quad (3)$$

where $\mu_{\ln IM}(M, R, \text{etc.})$ represents the mean of $\ln IM$ estimated by using $M, R, \text{etc.}$; $\sigma_{\ln IM}$ denotes the standard deviation of $\ln IM$ given by GMM; $\varepsilon_{\ln IM}$ is a standard normal variable. Based on the joint normal distribution of $\ln IM$ s, the N_{IM} samples can be readily generated by specifying the correlation coefficients among IM s (e.g., [12]).

- (v) Substitute each sample of IM (or IM s) into Eq. (1) (or Eq. (2)) to derive $\mu_{\ln D}$, and then perform MCS to generate N_D samples of D based on the distribution of $\ln D$. This process is repeated for N_{IM} times, resulting in $N_{IM} \times N_D$ data points of D .

3 Slope Model Establishment

Figure 1 shows the slope model established in the finite difference code *FLAC* [13], where the slope height (H) and slope angle are 20 m and 30° , respectively. The cyclic soil behavior is described by the hysteretic damping model Sig4, in which the model parameters are calibrated according to the Darendeli [14] modulus reduction and damping ratio curves with plasticity index of 0 and the effective vertical stress at the depth of H . Sig4 is combined with the Mohr-Coulomb plasticity criterion for modelling the plastic behavior of soils. To remove high-frequency noises, a small amount of stiffness-proportional Rayleigh damping (0.2%) is specified. The bedrock layer is considered linear-elastic with 0.5% mass- and stiffness-proportional Rayleigh damping. Table 1 summarizes the parameters assigned to the slope model. To minimize wave reflection effects, the quiet boundary is applied along the bedrock base, and the free-field boundary that simulates a quiet boundary is implemented at both lateral sides [13]. The sum of L_1 and L_2 is equal to $12H$, as illustrated in Fig. 1.

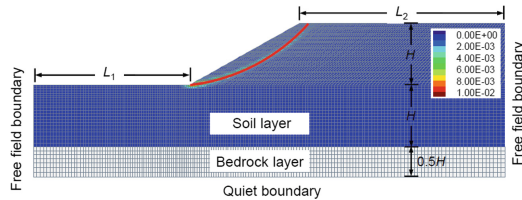


Fig. 1. Numerical model of slope and the associated maximum shear strain increment contours obtained from pseudostatic strength reduction technique. The CSS from Bishop's simplified method is shown using a red line.

Table 1. Summary of the geotechnical parameters assigned to the slope model.

Soil layer				Bedrock layer	
ρ (kg/m^3)	c (kPa)	ϕ ($^\circ$)	G_{\max} (MPa)	ρ (kg/m^3)	G_{\max} (MPa)
2000	10	35	320	2300	1472

Note: $\rho, c, \phi,$ and G_{\max} denote the density, cohesion, friction angle, and initial shear modulus of soil, respectively.

Before conducting dynamic analysis, pseudostatic slope stability analysis is conducted using both the strength reduction technique (SRT) and Bishop’s simplified limit equilibrium method. As also shown in Fig. 1, the resulting shear band from SRT agrees well with the critical slip surface (CSS) from the Bishop method. The fundamental period of the failure mass (above CSS) is estimated as $T_{s,mass} = 4h/V_s = 0.077$ s, where V_s is the soil shear-wave velocity (i.e., $V_s = \sqrt{G_{max}/\rho}$), and h denotes the maximum thickness of the failure mass. The fundamental period of the soil layer ($T_{s,layer}$) is similarly calculated using $h = 1.5H$ (average of the downhill and uphill soil layer thicknesses). In the next section, two degraded periods determined as $T_{d1} = 1.5T_{s,mass} = 0.116$ s and $T_{d2} = 1.5T_{s,layer} = 0.45$ s will be considered to construct the spectral acceleration (SA) for predicting earthquake-induced slope displacements (e.g., [2]).

4 Development of Slope-Specific Displacement Models

4.1 Construction of Displacement Models

The NGA-West2 database (<https://ngawest2.berkeley.edu/>) is used to select 83 GM records, which cover a wide range of peak ground acceleration (PGA) from 0.05 g to 1.41 g, allowing for a proper consideration of the GM record-to-record variability. Following Step (ii) in Sect. 2, the D for each GM is calculated as the maximum horizontal displacement along the slope surface.

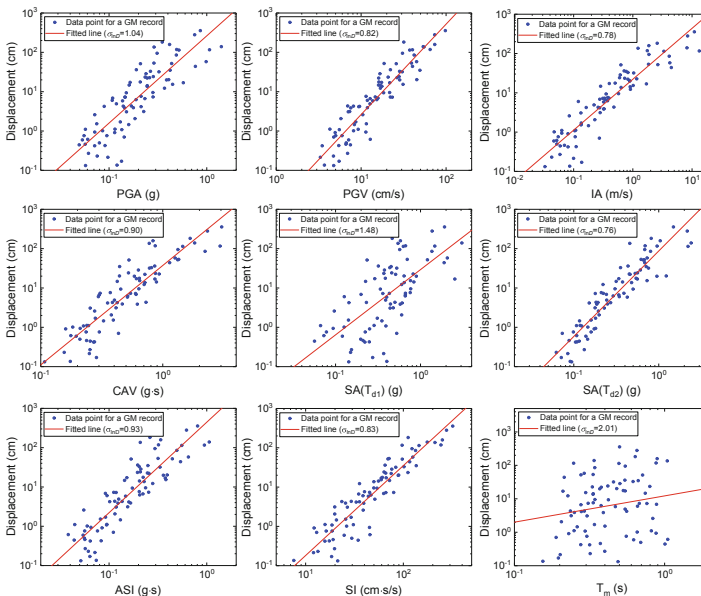


Fig. 2. Distribution of D versus different IMs. Also shown are trends fitted by Eq. (1) or (2).

For a thorough comparison, this study incorporates 10 representative IMs, including PGA, peak ground velocity (PGV), Arias intensity (IA), cumulative absolute velocity

(CAV), SA(T_{d1}), SA(T_{d2}), acceleration spectrum intensity (ASI), spectrum intensity (SI), mean period (T_m), and significant duration D_{s5-75} . Among them, SA(T_{d1}) and SA(T_{d2}) represent the 5%-damped spectral accelerations at the periods T_{d1} and T_{d2} , respectively. Note that most of the existing Newmark-type models correlate SA(T_{d1}) to D . Step (iii) is conducted for the 10 scalar IMs and 38 combinations of IMs, resulting in 48 D models.

Figure 2 shows the D versus IM distributions for 9 scalar IMs and the fitted linear trends (and the associated $\sigma_{\ln D}$). It is found that the $\ln D$ versus $\ln IM$ relationship generally follows a linear pattern. The SA(T_{d2}) model fits the data better than the others; yet, the more usually used SA(T_{d1}) leads to much larger scatter (i.e., $\sigma_{\ln D}$ is almost double). Also, the scatter for T_m and D_{s5-75} is significantly larger, indicating the low efficiency of the two scalar IMs in predicting D . Such wide ranges of D and IMs imply the capabilities of the models for estimating D in various shaking levels.

4.2 Standard Deviations of the Displacement Models

Figure 3a and b further compare $\sigma_{\ln D}$ for the scalar-IM and vector-IM models, respectively. The order of SA(T_{d2}) > IA > PGV > SI > CAV > ASI > PGA > SA(T_{d1}) > T_m > D_{s5-75} is observed for the efficiency of scalar IMs. The smallest $\sigma_{\ln D}$ of 0.76 for SA(T_{d2}) may be attributed to that $T_{d2} = 0.45$ s (for the soil layer’s fundamental period) is comparable to the value of T_m (e.g., see Fig. 2) and is more related to the dynamic response of the slope. This indicates that the degraded period for the failure mass (i.e., T_{d1}) should be used cautiously with the consideration of GMs’ period range. Besides, IA and PGV, which were identified as the two most efficient IMs by Cho and Rathje [8], yield similar $\sigma_{\ln D}$ (0.78 and 0.82) to that of SA(T_{d2}). Hence, the three IMs may be preferred for deriving D models. Although it is not a common IM, SI also results in relatively small $\sigma_{\ln D}$ (≈ 0.8). On the other hand, T_m and D_{s5-75} lead to significantly large $\sigma_{\ln D}$ (≈ 2).

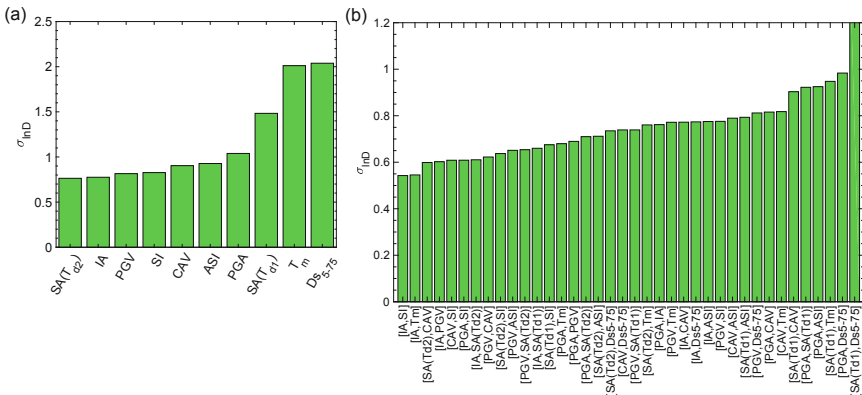


Fig. 3. Model-specific standard deviations for different (a) scalar-IM and (b) vector-IM models.

It is observed from Fig. 3b that the vector-IM models yield much smaller $\sigma_{\ln D}$ than the scalar-IM models as a result of more complementary information carried by two IMs. The

order of $[IA,SI] > [IA,T_m] > [SA(T_{d2}),CAV] > [IA,PGV] > [CAV,SI]$ is observed for the five most efficient vectors (i.e., $\sigma_{\ln D} = 0.54\text{--}0.61$). Specifically, the $\sigma_{\ln D}$ values (0.54 and 0.55) for $[IA,SI]$ and $[IA,T_m]$ are noticeably smaller, indicating the attractiveness of the two vectors. The $[SA(T_{d2}),CAV]$, $[IA,PGV]$, $[CAV,SI]$, $[PGA,SI]$, $[IA,SA(T_{d2})]$ and $[PGV,CAV]$ are the subsequently efficient vectors that achieve comparative $\sigma_{\ln D}$ within the range of 0.60–0.61. These vectors include either IA or CAV, which capture multiple characteristics (amplitude, duration, etc.) of GMs.

5 Scenario-Based Comparison of the Models Using MCS

Following Step (iv), the mean and variability of the D prediction for different models are compared under some representative scenarios. Multiple GMMs are adopted for individual IMs [11, 15–18] following the logic tree method. The correlation coefficient matrix for modeling the joint distribution of the 10 IMs is derived according to the references [12, 19, 20]. Both N_{IM} and N_D are specified as 200, yielding 40000 displacement values. The geometric mean of these values (termed as D_{mean} hereafter) and the standard deviation of $\ln D$ (St.d. of predicted $\ln D$) are investigated as follows.

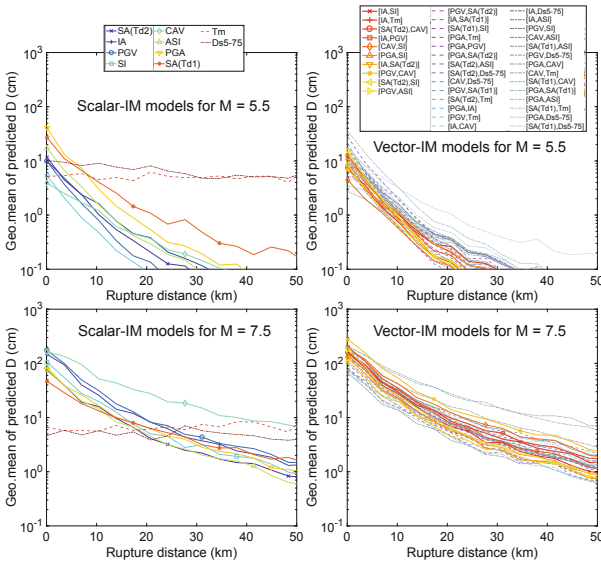


Fig. 4. Mean prediction trends associated with different displacement models for $V_{S30} = 760$ m/s

5.1 Mean of the Displacement Prediction

Figure 4 shows the D_{mean} versus R for $V_{S30} = 760$ m/s. Both $M = 5.5$ and 7.5, and the scalar- and vector-IM models are included. Note that the legend is shown in the way of illustrating the ranking of $\sigma_{\ln D}$ for different displacement models. The results

for $V_{S30} = 360$ m/s are not shown due to the limited space, yet are also discussed as follows. First, D_{mean} decreases with increasing R , while the decreasing trend becomes slower for larger R . Second, the trends for the scalar- and vector-IM models are generally comparable, and the difference of the results for most vector-IM models (especially for the 10 most efficient ones) is smaller in comparison with the scalar-IM models. Third, the model-to-model difference is slightly dependent on V_{S30} and M . Regarding the soil site condition ($V_{S30} = 360$ m/s), $M = 5.5$ generally corresponds to smaller difference of D_{mean} than $M = 7.5$; yet, this observation appears to reverse for the rock site condition. Fourth, the SA(T_{d1}) model generally produces the upper and lower bounds among the scalar-IM models for $M = 5.5$ and 7.5 , respectively. The T_m and DS_{5-75} models are two exceptional cases with almost unchanged D_{mean} , indicating that the two IMs should not be used solely to predict D .

5.2 Variability in the Displacement Prediction

Figure 5 displays the St.d. of predicted $\ln D$ versus R for $V_{S30} = 760$ m/s. The $V_{S30} = 360$ m/s case produces slightly smaller St.d., and is not shown here for brevity. No evident trend of St.d. versus R is observed. The St.d. values for the scalar-IM models are generally comparable to those for the vector-IM models, although the 10 most efficient vector-IM models tend to result in smaller St.d. values. As a superposition of $\sigma_{\ln IM}$ and $\sigma_{\ln D}$, St.d. is generally within the range from 1.4 to 1.8.

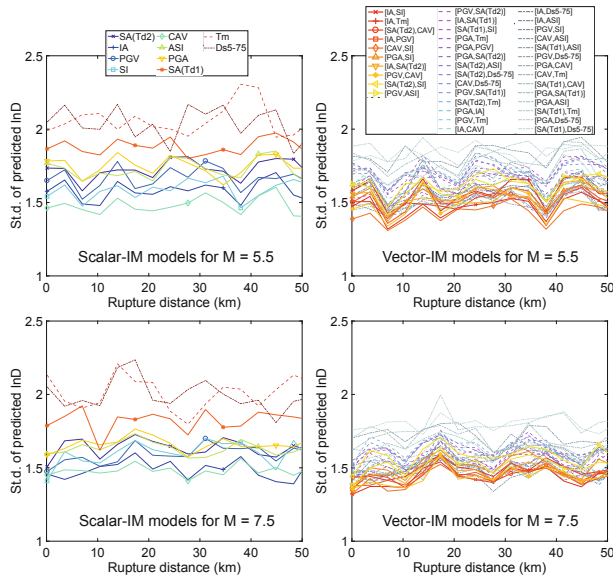


Fig. 5. Variability trends associated with different displacement models for $V_{S30} = 760$ m/s.

For comparison, Table 2 lists the different types of standard deviations for the scalar-IM models, where μ_{Std} represents the average of St.d. for different scenarios (various

V_{S30} and R). It is seen that the IM for the smallest μ_{Std} may not produce the smallest $\sigma_{\ln D}$, due to the additionally included uncertainty in the IM prediction. In general, CAV tends to yield smaller μ_{Std} , and μ_{Std} for IA is still relatively small. The μ_{Std} values for the 38 vector-IM models are derived and are shown in Fig. 6. A similar observation of different rankings of μ_{Std} and $\sigma_{\ln D}$ can be made. Specifically, the low uncertainty in estimation of CAV is illustrated again; that is, some IM vectors including CAV yield relatively small total variability (μ_{Std}). The larger μ_{Std} is, the more uncertain the displacement prediction. Though $\sigma_{\ln D}$ can generally be smaller than 0.75, the total uncertainty is still large, and in most cases μ_{Std} has exceeded 1.4. Take the predicted D of 40 cm given an earthquake scenario as an example; the expected range of D considering the total uncertainty ($\mu_{Std} = 1.4$) can be estimated as $[\exp(\ln(40) - \mu_{Std}), \exp(\ln(40) + \mu_{Std})] = [10 \text{ cm}, 162 \text{ cm}]$ [2]. Such a large interval should be shrunk for a more robust estimation of D . Thus, more powerful GMMs with smaller aleatory variability should be developed and applied to the seismic slope displacement analysis.

Table 2. Standard deviation parameters for the scalar-IM models.

IM ₁	$\sigma_{\ln IM} (M = 5.5)$	$\sigma_{\ln IM} (M = 7.5)$	$\sigma_{\ln D}$	$\mu_{Std} (M = 5.5)$	$\mu_{Std} (M = 7.5)$
PGA	0.58–0.65	0.52–0.58	1.04	1.73	1.63
PGV	0.63–0.64	0.59–0.60	0.82	1.67	1.58
IA	1.01–1.08	0.94–0.99	0.78	1.57	1.46
SA (T _{d1})	0.59–0.71	0.54–0.64	1.48	1.86	1.79
SA (T _{d2})	0.66–0.69	0.61–0.64	0.76	1.72	1.62
CAV	0.39–0.49	0.39–0.43	0.90	1.46	1.42
SI	0.60–0.62	0.60–0.61	0.83	1.59	1.60
ASI	0.56–0.63	0.52–0.57	0.93	1.71	1.60

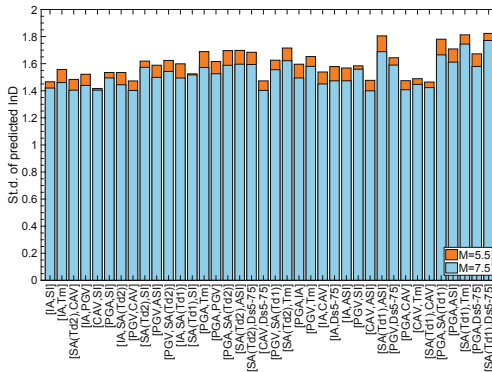


Fig. 6. Comparison of μ_{Std} for different vector-IM displacement models.

6 Summary and Conclusions

This study investigated the relationship between ground motion intensity measures (IMs) and earthquake-induced permanent slope displacement (D) based on numerical stress-deformation analyses. Ten scalar IMs and 38 vector-IM combinations, were used to develop the D models, and the efficiencies of various scalar and vector-IMs were compared in terms of the model standard deviation ($\sigma_{\ln D}$). Furthermore, a Monte Carlo simulation-based procedure was utilized to compare these D models under representative earthquake scenarios, in which the uncertainties in predicting both IMs and D are considered. The comparative results lead to the following conclusions:

1. The SA($T_{d2} = 1.5T_{s, \text{layer}}$)- and IA-based displacement models were identified as the most efficient scalar-IM models with the smallest $\sigma_{\ln D}$ of 0.77, while the more commonly used SA($T_{d1} = 1.5T_{s, \text{mass}}$) resulted in much larger $\sigma_{\ln D}$. In contrast, the scalar IMs of T_m and DS_{5-75} exhibit the lowest efficiency in regressing D .
2. The [IA,SI] and [IA, T_m] resulted in the smallest $\sigma_{\ln D}$ of about 0.55 for the vector-IM models. The subsequent six most efficient models generally included either IA or CAV. Only 6 among the 38 models yielded $\sigma_{\ln D}$ greater than 0.77, indicating the advantage of vector-IM models for improving the efficiency of regressing D .
3. The total standard deviation contributed by both the uncertainties in IM and D predictions is considerably larger than $\sigma_{\ln D}$, and the models with the smallest $\sigma_{\ln D}$ do not necessarily yield the smallest total standard deviation. This is more evident for models including CAV in which a smaller variability is involved in predicting this IM. Recent studies on developing non-ergodic ground motion models shed light in the direction of reducing variability in the IM prediction (e.g., [21]).

The results of the mean and standard deviation of D obtained in this study could be useful to select IMs in developing predictive models for seismically-induced slope displacements. Such models can be implemented within the fully-probabilistic framework [7, 8], allowing practitioners to estimate the hazard-compatible D for seismic design of slopes.

References

1. Newmark, N.M.: Effects of earthquakes on dams and embankments. *Geotechnique* **15**(2), 139–160 (1965)
2. Bray, J.D., Travasarou, T.: Simplified procedure for estimating earthquake-induced deviatoric slope displacements. *Journal of Geotechnical and Geoenvironmental Engineering* **133**(4), 381–392 (2007)
3. Du, W., Huang, D., Wang, G.: Quantification of model uncertainty and variability in Newmark displacement analysis. *Soil Dyn. Earthq. Eng.* **109**, 286–298 (2018)
4. Jibson, R.W.: Methods for assessing the stability of slopes during earthquakes—A retrospective. *Eng. Geol.* **122**(1–2), 43–50 (2011)
5. Rathje, E.M., Saygili, G.: Probabilistic seismic hazard analysis for the sliding displacement of slopes: scalar and vector approaches. *Journal of Geotechnical and Geoenvironmental Engineering* **134**(6), 804–814 (2008)

6. Li, D.Q., Wang, M.X., Du, W.: Influence of spatial variability of soil strength parameters on probabilistic seismic slope displacement hazard analysis. *Engineering Geology* 105744 (2020)
7. Wang, M.X., Li, D.Q., Du, W.: Probabilistic seismic displacement hazard assessment of earth slopes incorporating spatially random soil parameters. *J. Geotechn. Geoenvironmen. Eng.* **147**(11), 04021119 (2021)
8. Cho, Y., Rathje, E.M.: Displacement hazard curves derived from slope-specific predictive models of earthquake-induced displacement. *Soil Dyn. Earthq. Eng.* **138**, 106367 (2020)
9. Wang, G.: Efficiency of scalar and vector intensity measures for seismic slope displacements. *Front. Struct. Civ. Eng.* **6**(1), 44–52 (2012)
10. Fotopoulou, S.D., Pitilakis, K.D.: Predictive relationships for seismically induced slope displacements using numerical analysis results. *Bull. Earthq. Eng.* **13**(11), 3207–3238 (2015). <https://doi.org/10.1007/s10518-015-9768-4>
11. Gregor, N., et al.: Comparison of NGA-West2 GMPEs. *Earthq. Spectra* **30**(3), 1179–1197 (2014)
12. Bradley, B.A.: A ground motion selection algorithm based on the generalized conditional intensity measure approach. *Soil Dyn. Earthq. Eng.* **40**, 48–61 (2012)
13. Itasca Consulting Group: FLAC-Fast Lagrangian analysis of continua. Version 8.0. User's manual (2016)
14. Darendeli, M.B.: Development of a new family of normalized modulus reduction and material damping curves. Ph.D. thesis. Dept. of Civil, Architectural and Environmental Engineering, Univ. of Texas at Austin (2001)
15. Campbell, K.W., Bozorgnia, Y.: Ground motion models for the horizontal components of Arias intensity (AI) and cumulative absolute velocity (CAV) using the NGA-West2 database. *Earthq. Spectra* **35**(3), 1289–1310 (2019)
16. Du, W., Wang, G.: A simple ground-motion prediction model for cumulative absolute velocity and model validation. *Earthquake Eng. Struct. Dynam.* **42**(8), 1189–1202 (2013)
17. Afshari, K., Stewart, J.P.: Physically parameterized prediction equations for significant duration in active crustal regions. *Earthq. Spectra* **32**(4), 2057–2081 (2016)
18. Rathje, E.M., Faraj, F., Russell, S., Bray, J.D.: Empirical relationships for frequency content parameters of earthquake ground motions. *Earthq. Spectra* **20**(1), 119–144 (2004)
19. Bradley, B.A.: Correlation of Arias intensity with amplitude, duration and cumulative intensity measures. *Soil Dyn. Earthq. Eng.* **78**, 89–98 (2015)
20. Du, W.: Empirical correlations of frequency-content parameters of ground motions with other intensity measures. *J. Earthquake Eng.* **23**(7), 1073–1091 (2019)
21. Abrahamson, N.A., Kuehn, N.M., Walling, M., Landwehr, N.: Probabilistic seismic hazard analysis in California using nonergodic ground-motion models. *Bull. Seismol. Soc. Am.* **109**(4), 1235–1249 (2019)